

Computer Validation of Neural Network Dynamics: A First Case Study

Kuehn, Christian* and Queirolo, Elena [†]

February 11, 2022

Abstract

A large number of current machine learning methods rely upon deep neural networks. Yet, viewing neural networks as nonlinear dynamical systems, it becomes quickly apparent that mathematically rigorously establishing certain patterns generated by the nodes in the network is extremely difficult. Indeed, it is well-understood in the nonlinear dynamics of complex systems that, even in low-dimensional models, analytical techniques rooted in pencil-and-paper approaches reach their limits quickly. In this work, we propose a completely different perspective via the paradigm of rigorous numerical methods of nonlinear dynamics. The idea is to use computer-assisted proofs to validate mathematically the existence of nonlinear patterns in neural networks. As a case study, we consider a class of recurrent neural networks, where we prove via computer assistance the existence of several hundred Hopf bifurcation points, their non-degeneracy, and hence also the existence of several hundred periodic orbits. Our paradigm has the capability to rigorously verify complex nonlinear behaviour of neural networks, which provides a first step to explain the full abilities, as well as potential sensitivities, of machine learning methods via computer-assisted proofs.

1 Introduction

Machine learning [1, 2, 3] has been an extremely dynamic field in recent years [4, 5]. Deep neural networks have taken center stage as a key algorithmic component [6, 7]. Although several results about static functional approximation properties of neural networks are quite classical [8, 9], studying their dynamics mathematically rigorously, i.e., to really *prove* that they generate a particular behaviour, still remains a formidable challenge. From an abstract viewpoint, this is not too surprising since the propagation of information across a neural network with fixed edge weights, as well as the learning process of the edge weights, are large-scale nonlinear dynamical systems [10, 11]. It is well-understood that if one seeks verified rigorous mathematical results about nonlinear dynamics, one usually has to make quite significant assumptions [12]. Examples of these assumptions are low dimensionality [13, 14], scale separation [15, 16], existence of a mean-field [17, 18], or a gradient structure [19, 20]. In fact, if these assumptions are missing, then already questions about very low-dimensional dynamics, say in dimensions one to three for iterated maps of flows, become almost impossible to solve via rigorous pencil-and-paper arguments [21]. Therefore, if we are interested in generic neural networks without simplifying assumptions, which are frequently the cases most relevant for many practical algorithms, it seems that we would have to abandon the hope to ever validate mathematically that modern machine learning algorithms behave correctly.

*ckuehn@ma.tum.de

[†]elena.queirolo@tum.de

In this work, we propose a completely new perspective to validation of neural network dynamics and thereby also to robustness and verification of artificial intelligence. The idea is to use automated computational tools to rigorously validate the dynamics of neural networks. Although this perspective might sound counter-intuitive at first, it can be well-founded within the field of numerical validation methods [22, 23, 24, 25]. In particular, viewing the neural network as a dynamical system, we are going to utilize and adapt computational techniques first developed to solve hard open problems in dynamics, probably most famously the existence of the Lorenz attractor [26]. The principle is that certain patterns, respectively solution behaviours, can be tackled numerically. The numerical solution is then verified rigorously via interval arithmetic error bounds in combination with a-priori or a-posteriori error estimates. This combination of techniques can indeed provide rigorous mathematical proofs for otherwise intractable global nonlinear dynamics. In the context of neural networks, it has the nice interpretation that we use a more classical computational approach in combination with theoretical mathematical bounds and computer-assisted error tracking to validate the existence of patterns in neural networks, which can then be used as an even more powerful computational tool.

Of course, implementing such an idea requires a longer term development and testing for various classes of deep neural networks. In this work, we are interested in a first proof-of-principle, i.e., to demonstrate how the idea of numerical validation can be brought to tackle intermediate size neural networks. As a test case, we study a well-established class of anti-symmetric recurrent neural networks (RNNs) [27], and we focus on the dynamics on the network for edge weight matrices with random weights to ensure robustness of our results. We show that in a generic setting and under the assumption of large depth, varying a main hyperparameter of the network leads to a whole cascade of Hopf bifurcations, where periodic solutions are generated. Via the so-called polynomial radii approach, we validate

several hundred Hopf bifurcations rigorously and we also compute the relevant first Lyapunov coefficient rigorously. We find that the generated periodic solutions are all unstable leading to a phase space structure for the neural network, where many transient oscillatory motions are possible. In fact, it is well-understood that within the class of all possible dynamical systems, looking for large classes of (unstable) periodic solutions is a strategy to determine the possible high complexity and potentially chaotic dynamics of the system. In summary, we have demonstrated rigorously that within the space of even varying a single hyperparameter, the considered class of RNNs has enormous dynamical complexity. More importantly, we have demonstrated a paradigm that can complement validating the dynamics of neural networks precisely in the regimes, where other, often quite strong, mathematical assumptions needed for purely analytical arguments break down.

The paper is structured as follows: in Section 2 an overview of the considered RNN is given, together with a first introduction to Hopf bifurcations. In Section 3, an algebraic problem is built for the search of Hopf bifurcations in a general ODE, then the problem of validating its results is discussed in Section 4. The results are then presented in Section 5. A brief outlook is given in Section 6. Two Appendices are given with details on the application of the radii polynomial approach to the RNN (Appendix A) and on the computation of the Lyapunov coefficient to prove non-degeneracy (Appendix B).

2 Bifurcations in AntisymmetricRNN

We are focusing on implementing the idea to use rigorous numerical validation for a class of neural networks known as antisymmetric recurrent neural networks (AntisymmetricRNN [27]). In this class of recurrent neural networks, the output layer $x_T \in \mathbb{R}^n$ is the result of applying a sequence of nonlinearities to the input layer $x_0 \in \mathbb{R}^n$, and each

hidden layer is determined by

$$x_t = x_{t-1} + \sigma(Wx_{t-1} + Vd_t + b), \\ t = 0, 1, \dots, T$$

where $x_t \in \mathbb{R}^n$ is the t -th hidden layer, $d_t \in \mathbb{R}^m$ is the input for the same layer, while $W \in \mathbb{R}^{n \times n}$, $V \in \mathbb{R}^{n \times m}$ and $b \in \mathbb{R}^n$ are parameters of the RNN. In practice, these parameters can depend on the layer, but in our exposition they will be fixed, i.e., we focus on the information propagation dynamics on the network and not on the learning step. W and V are called weights, while b is the bias. It is possible to vary the dimensions n and m along the layers, but we will not make use of such flexibility for this first case study. In [27], a concrete subclass of RNNs is studied given by

$$x_t = x_{t-1} + \varepsilon \tanh(\hat{W}x_{t-1} + Vd_t + b), \quad (1)$$

where

$$\hat{W} \stackrel{\text{def}}{=} W - W^\top + \gamma \text{Id},$$

and $\varepsilon \in \mathbb{R}$ and $\gamma \in \mathbb{R}$ are hyperparameters, and Id is the identity matrix. Here the hyperbolic tangent acts element-wise. One may view equation (1) as the application of the Euler method to the ordinary differential equation (ODE)

$$x'(t) = \tanh(\hat{W}x(t) + Vd(t) + b), \quad (2)$$

where we now consider x to be an n -dimensional function of continuous time $t \in [0, T]$. The value of x_t at the input and output layers of the RNN are equivalent to the values of $x(t)$ at $t = 0$ and $t = T$.

Studying the dynamics induced by (2) is a powerful tool in understanding the effects the RNN has on its input vector.

Bifurcations provide insight on the global behaviour of a system through a local study, so they are a fitting starting topic. We are particularly interested in studying the bifurcations this dynamical system can exhibit depending on the hyperparameters after the weights and bias have been determined during the learning phase of the RNN. In particular, following the presentation in [27], we want to determine when the system can undergo a Hopf bifurcation. Hopf bifurcations

are one of the mechanisms for the appearance of periodic orbits, a topic of interest in its own right. Hopf bifurcations happen when a pair of imaginary eigenvalues of the Jacobian crosses the imaginary axes with non-zero velocity. We refer to Definition 1 for additional details on their mathematical structure. In this section, we first justify that γ is the hyperparameter of interest, when searching for Hopf bifurcations in (2).

In order to simplify the explanation, we consider no input data over time, i.e. $d(t) = 0$. The unique zero of the hyperbolic tangent is at zero, so the non-linearity simplifies and we retrieve the algebraic problem

$$\hat{W}x(t) + b = 0.$$

For simplicity, and without loss of generality, we restrict ourselves additionally by setting the bias to zero, $b = 0$. In this case, an important equilibrium of the n -dimensional system is the trivial equilibrium $x_\star = 0$. The Jacobian of (2) is

$$J(x) = (\text{Id} - \text{diag}(\tanh(\hat{W}x(t)))^2)\hat{W}, \quad (3)$$

where the power is considered element-wise and $\text{diag}(\cdot)$ is the diagonal matrix obtained from a vector. Computing the Jacobian at x_\star , the hyperbolic tangent vanishes, leaving us with

$$J(x_\star) = \hat{W}.$$

Thus, studying the behaviour of the Jacobian at the equilibrium is equivalent to studying \hat{W} . We notice that the eigenvalues of anti-symmetric matrices, such as $W - W^\top$ are imaginary. Since \hat{W} is a shift by γ of an anti-symmetric matrix, the real part of all eigenvalues of \hat{W} is equal to γ . In particular, all eigenvalues of \hat{W} cross the imaginary axes for γ crossing zero. This creates a highly degenerate Hopf bifurcation at $\gamma = 0$.

Remark 1. Imaginary eigenvalues appear in pairs, thus antisymmetric matrices of odd size must have a real eigenvalue, and it must be 0. Consequently, antisymmetric matrices of odd size are singular and in particular, at $\gamma = 0$, \hat{W} is singular.

Considering practical applications, where \hat{W} is computed from data, we can expect \hat{W} to include a small not anti-symmetric perturbation P , such as

$$\hat{W}(\gamma) = W - W^\top + \gamma \text{Id} + P, \quad (4)$$

where the dependence on γ is now made explicit and where we expect P to be small in a suitable matrix norm. It is expected that a generic small perturbation is sufficient to make the degeneracy disappear. Then, pairs of eigenvalues would still cross the imaginary axes, but not at the same values of γ . This can generate a finite cascade of Hopf bifurcations for γ close to 0. Additionally, a perturbation would ensure that the Jacobian is non-singular at all values of γ , including odd-dimensional problems at $\gamma = 0$.

In summary, we now have an ODE representing an RNN, such that one hyperparameter could be responsible for a cascade of Hopf bifurcations. With such initial understanding in mind, we delve deeper into the search for Hopf bifurcations, and describe them from a more general perspective.

It is worth remarking that the following two sections are presented in an abstract setting and can be applied to a variety of RNNs. The code presented in [28] is mostly general, and the modifications to apply it to a new system only include the definition of the system and its derivatives.

3 Algebraic Hopf bifurcation

In the previous Section 2, the possibility of having Hopf bifurcations appearing in the RNN (2) was presented. In this section, we discuss the numerical search for such bifurcations, by introducing the zero finding problem associated to Hopf bifurcations. For additional flexibility, the discussion below is going to be framed in a more general setup, treating a generic parameter dependent ODE system of the form $x' = f(x, \gamma)$, where γ is a real parameter. In such ODEs, a non-degenerate Hopf bifurcation is the pair (x_*, γ_*) at which a periodic orbit bifurcates from an equilibrium.

Definition 1. A Hopf bifurcation (x_*, γ_*) of $x' = f(x, \gamma)$ is such that (x_*, γ_*) is an equilibrium of the ODE, i.e. $f(x_*, \gamma_*) = 0$, such that $D_x f(x_*, \gamma_*)$ has a pair of purely imaginary eigenvalues $\lambda_*, \bar{\lambda}_*$. Furthermore, the Hopf bifurcation is non-degenerate if there are no other imaginary eigenvalues of $D_x f(x_*, \gamma_*)$ and λ_* crosses the imaginary axis with non-zero velocity w.r.t. γ at $\gamma = \gamma_*$.

Setting momentarily aside the non-degeneracy conditions, we can set the algebraic problem as

$$\begin{cases} f(x, \gamma) = 0, \\ D_x f(x, \gamma)v - \lambda v = 0, \end{cases} \quad \lambda \in \mathbf{i}\mathbb{R}.$$

Notice how the eigenvalue v is defined just up to a scaling, thus an additional equation involving the normalization of v needs to be included to guarantee uniqueness of the solution. We define all solutions of this problem as *algebraic Hopf bifurcations*. Such bifurcations might be degenerate.

While the algebraic Hopf problem is mathematically well-posed, up to a complex rescaling of v , it is defined on the space $(x, \gamma, v, \lambda) \in (\mathbb{R}^n, \mathbb{R}, \mathbb{C}^n, \mathbf{i}\mathbb{R})$. It is numerically cumbersome to impose that the solution exactly fits into the appropriate space, since it mixes real, complex and imaginary values. Instead of solving it directly, we rephrase the problem into a fully real space. We introduce the notation $v = v_r + \mathbf{i}v_i$ and $\lambda = \mathbf{i}\lambda_i$, where now $v_r, v_i \in \mathbb{R}^n$ and $\lambda_i \in \mathbb{R}$. We also add two equations

$$\phi^\top v_r = 0 \quad \phi^\top v_i - 1 = 0,$$

where ϕ is any fixed vector in \mathbb{R}^n , to fix the scaling of v_r and v_i . Then, we write the real algebraic Hopf problem as

$$\begin{cases} \phi^\top v_r = 0, \\ \phi^\top v_i - 1 = 0, \\ f(x, \gamma) = 0, \\ D_x f(x, \gamma)v_r + \lambda_i v_i = 0, \\ D_x f(x, \gamma)v_i - \lambda_i v_r = 0. \end{cases} \quad (5)$$

With the addition of this scaling, the problem is numerically well-posed and has, generically, a locally unique solution.

Equation (5) is now real and finite dimensional, any root finding algorithm, such as Newton's method, can be used to find its numerical solutions. This yields numerical approximations of algebraic Hopf bifurcations. A discussion on the initialization of such root finding algorithms can be found in Remark 3.

Having computed a numerical solution to the algebraic Hopf problem, an overview of its validation is given in Section 4, while details pertaining to its practical implementation are presented in Appendix A. The problem of proving non-degeneracy is discussed at the end of the Section 4, while details of its computation are presented in Appendix B.

4 Validation in finite dimensions

In this section, an *a-posteriori* method of validation for zero-finding problems is presented. Following, among others, [29, 30], we will give here an overview of the radii polynomial approach.

Consider (5) as a zero-finding problem $F(x) = 0$, where $F : X \rightarrow Y$ and X, Y are Banach spaces with norms $\|\cdot\|_X, \|\cdot\|_Y$. For concreteness, one may think of finite-dimensional Euclidean spaces X, Y here but the validation idea works in more generality, even in infinite-dimensional settings, so we keep this generality in the presentation to make it evident, how far-reaching the approach actually is. If \tilde{x} is close enough to a solution of the zero-finding problem, we expect the Newton operator $\tilde{x} - DF(\tilde{x})^{-1}F(\tilde{x})$ to be contracting towards the exact solution. Based on this intuition, we define the map

$$\begin{aligned} T : X &\rightarrow X \\ x &\mapsto x - AF(x), \end{aligned} \quad (6)$$

where $A : Y \rightarrow X$ is an approximation of $DF(\tilde{x})^{-1}$. We set out to prove that T is a contraction. More precisely, with the radii polynomial approach, we prove the existence of an r such that the approximate Newton operator T is a contraction in the ball $B_r(\tilde{x})$ of radius r around the numerical

solution \tilde{x} . This yields a rigorous existence of a zero very close to the numerically computed one \tilde{x} . With this strategy in place, we can now present the radii polynomial theorem from [31].

Theorem 1. *Let T be as defined in (6) and let*

$$\begin{aligned} Y &\geq \|T(\tilde{x})\|_X, \\ Z(r) &\geq \sup_{b,c \in B_1(0) \subset X} \|DT(\tilde{x} + rb)rc\|_X. \end{aligned}$$

The radii polynomial is

$$p(r) \stackrel{\text{def}}{=} Y + Z(r) - r.$$

If there is a $r_\star > 0$ such that $p(r_\star) = Y + Z(r_\star) - r_\star < 0$ then T is a uniform contraction on $B_{r_\star}(\tilde{x})$. If A is non-singular, then F has a unique zero in $B_r(\tilde{x})$

The application to our finite dimensional system is presented in the Appendix A. Since the bounds need to be themselves rigorously computed, interval arithmetic is necessary.

Remark 2. To ensure the correctness of the bounds, all numerical errors need to be considered, such as rounding errors in the computation of the hyperbolic tangent and floating point errors. Interval arithmetic is the tool used to keep track of such errors, the used implementation in Matlab is the Intlab library, [32].

Once the solution to (5) is validated, we have proven the existence of an algebraic Hopf bifurcation, but we do not yet have knowledge of its non-degeneracy. For a non-degenerate bifurcation, we need to satisfy the two non-degeneracy conditions, as in Definition 1. The first one is the lack of other imaginary eigenvalues. Considering a finite dimensional system, this condition can be checked directly, by computing all other eigenvalues and confirming that their real part is non-zero. Validation of eigenvalues is a built-in functionality in Intlab and to prove this condition is straightforward.

The second condition for non-degeneracy is for the imaginary eigenvalue pair to be crossing the imaginary axes with non-zero velocity w.r.t. the parameter. This condition is more

technical and it is equivalent to the first Lyapunov coefficient being non-zero, as presented in [33]. To discuss the computation and validation of the first Lyapunov coefficient in our situation, we refer the interested reader to Appendix B.

5 Results

We apply the rewriting (5) of the Hopf bifurcation to equation (2), thus retrieving an algebraic Hopf problem of the form

$$\begin{aligned} F(y) &= F(x, \gamma, v_r, v_i, \lambda_i) \\ &= \begin{pmatrix} \phi^\top v_r \\ \phi^\top v_i - 1 \\ \tanh(\hat{W}(\gamma)x) \\ \partial_x(\tanh(\hat{W}(\gamma)x))v_r + \lambda_i v_i \\ \partial_x(\tanh(\hat{W}(\gamma)x))v_i - \lambda_i v_r \end{pmatrix} \\ &= 0, \end{aligned} \quad (7)$$

where $F : \mathbb{R}^{3n+2} \rightarrow \mathbb{R}^{3n+2}$. Following the discussion in Section 2, we focus on the zero of $\tanh(\hat{W}(\gamma)x)$ happening at $x = 0$ for all γ . This simplifies $\partial_x(\tanh(\hat{W}(\gamma)x)) = \tanh'(\hat{W}(\gamma)x)\hat{W}(\gamma) = \hat{W}(\gamma)$. The Jacobian then has $\lfloor n/2 \rfloor$ pairs of complex eigenvalues, each pair crossing the imaginary axis at some value of γ , likely close to 0. We consider then each pair of eigenvalues $\lambda_j, j = 1, \dots, n/2$ as a function of γ . For each pair of eigenvalues, we search for the bifurcation value γ_j , such that $\lambda_j(\gamma_j)$ is purely imaginary. Then, we validate the existence of an algebraic Hopf bifurcation at $(x, \gamma) = (0, \gamma_j)$. We also study the other eigenvalues of $\hat{W}(\gamma_j)$ to ensure that no other eigenvalue is crossing the imaginary axis at the same value γ_j . After computing the first Lyapunov coefficient and ensuring that it is different from 0, we have completed the validation of Hopf bifurcations. Furthermore, it is possible to check the sign of the first Lyapunov coefficient to confirm the stability of the periodic orbit generated at the Hopf bifurcation. All run validations returned a positive Lyapunov exponent, determining that the bifurcating branch of periodic solutions is unstable.

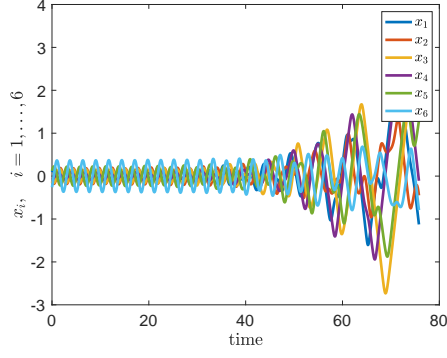
5.1 Hopf validation for RNNs

We now provide the details for the concrete validation for our model problem. We define $\hat{W}(\gamma)$ as in (4), where W and P are two random square matrices whose values are taken from a normal distribution. For our code, it is possible to give as input (to `asym_RHS_Hopf`) the seed for the random number generator and the amplitude of the perturbation, thus defining both W and P .

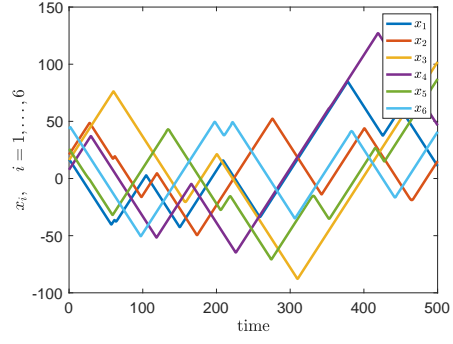
For a wide array of problems, with dimensions ranging from 2 to 400, the code provided in [28] numerically computes the existence of a solution to the algebraic Hopf problem (5), validates the algebraic Hopf problem following the procedure in Appendix A and computes the validated first Lyapunov coefficient as in Appendix B. In Figure 1, some visual results are presented. Each plot represents (some coordinates of) an orbit close to the Hopf bifurcation. In the first column of Figure 1, transient behaviour is presented. In all cases computed, all Lyapunov coefficients are positive, thus the periodic orbits created by the Hopf bifurcations are unstable. Still, it is usually possible to numerically shadow them for a short period of time. This is achieved by starting a forward integration at an approximate periodic orbit. The second column of Figure 1 presents an orbit at the same parameter γ close to the Hopf bifurcation, but the initial condition is chosen far away from the periodic orbit. This gives a graphical comparison between an orbit initially shadowing periodicity, and generic orbit at the same parameter value. The parameter value chosen is slightly larger than the largest γ_j .

The validation algorithm is very robust, and succeeds in validating most numerically found Hopf bifurcations. For example, in the 400 dimensional case presented, 200 Hopf bifurcations are found numerically and 198 are validated.

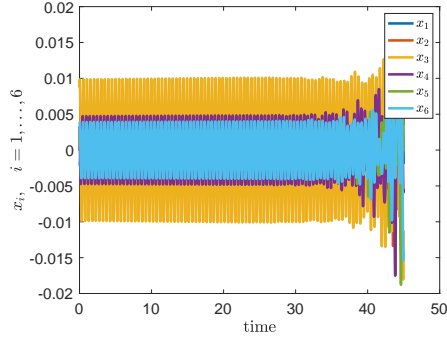
Rarely, the random \hat{W} created can be singular at a Hopf bifurcation. If this is the case, the validation of the algebraic Hopf problem fails. An example of an orbit in such a case is presented in Figure 2, where the orbit initially stays close to an unstable singular equilibrium



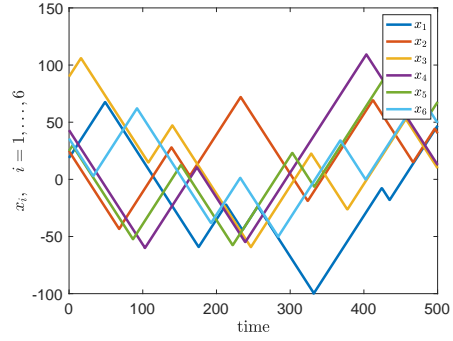
(a) Transient dynamics in 6 dimensions, $\gamma = 0.025848$



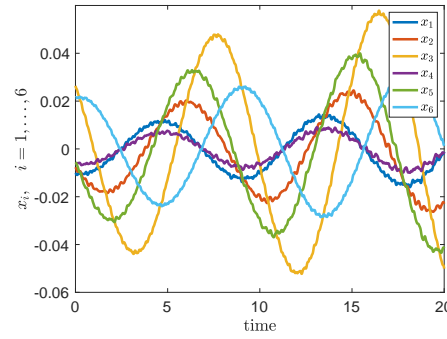
(b) Another orbit in 6 dimensions for the same parameter value



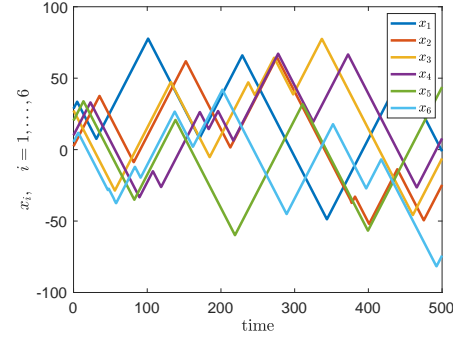
(c) Transient dynamics in 50 dimensions, $\gamma = 0.193188$



(d) Another orbit in 50 dimensions for the same parameter value



(e) Transient dynamics in 400 dimensions, $\gamma = 0.201686$



(f) Another orbit in 400 dimensions for the same parameter value

Figure 1: For a fixed parameter γ close to a Hopf bifurcation, transient dynamics is compared to a random orbit in 6, 50 and 400 dimensions. For these computations, the matrices W and P are set as randomly generated matrices, each element is i.i.d. in $\mathcal{N}(0, 1)$ and $\mathcal{N}(0, 0.1)$ respectively. The seed for the random number generator is set to 80. In the interest of clarity, only the first 6 coordinates are plotted with respect to time.

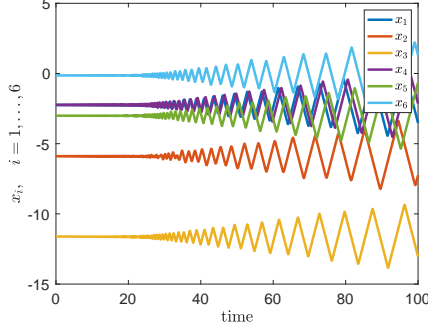


Figure 2: Non-validated algebraic Hopf bifurcations often show unusual behaviours close to the bifurcation parameter. For 50 dimensions, and the random seed set at 120, the validation of one of the Hopf bifurcations fails during the validation of the numerical solution of the algebraic Hopf problem. In this case, the transient dynamics is not periodic, but stationary. The parameter is $\gamma = 0.188821$.

point before diverging.

All figures can be created running `figure_generation.m`.

5.2 Numerical comparison

To study more in depth the creation of new periodic orbits, we also wanted to understand, whether the branches of periodic orbits match purely numerical results (i.e. without validation) that can be obtained with numerical continuation software. We have used MatCont [34], which provides a nice cross-benchmark. For this comparison, we started with the system

$$\begin{cases} x' = -\tanh((0.1\gamma + 0.0929)x + 1.4109y \\ \quad - 0.6359z - 1.6482w), \\ y' = -\tanh(-1.3993x + (0.1\gamma + -0.0672)y \\ \quad + 0.8243z + 0.7872w), \\ z' = -\tanh(0.7769x - 0.7604y + (0.1\gamma \\ \quad + 0.0325)z + 1.8087w), \\ w' = -\tanh(1.4191x - 0.8182y - 1.7241z \\ \quad + (0.1\gamma + 0.0373)w), \end{cases} \quad (8)$$

where the initial matrices were created at random, and the Hopf bifurcations were val-

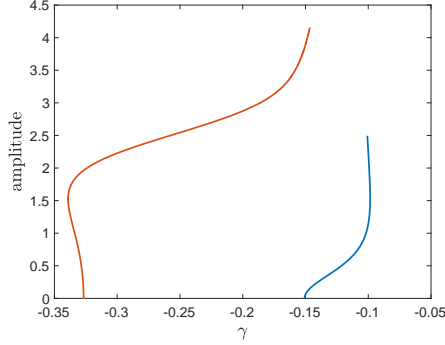
idated before the rescaling of the parameter γ . The rescaling was implemented to increasingly separate the two Hopf bifurcations. For these parameters, the bifurcation diagram is depicted in Figure 3a. The Hopf bifurcations computed with MatCont agree with the rigorously validated ones. The global continuation of the periodic orbit branches is purely numerical, and can be achieved with MatCont [34]. Validation of periodic orbits starting from a Hopf bifurcation is a topic presented in [35]. The full presentation of these techniques is not within the scope of this article, and we refer the interested read to [35] for an overview of validation of periodic orbits generated from Hopf bifurcations in polynomial vector fields. In our case, the vector field is non-polynomial and automatic validation techniques need to be applied, such as the ones presented in [30] and [36].

In a similar way, larger ODE systems can be studied, where the bottleneck resides mainly in computational time. In this way, a 20 dimensional system has been studied, the code presented in `validation_2.matcont.m`. It was possible to validate 10 Hopf bifurcations, as expected from a 20 dimensional system, but MatCont was able to find only 9 of them, mainly due to bifurcations being very close to one-another. If properly initialised, MatCont could recognise the validated bifurcations as Hopf bifurcations. The full bifurcation diagram is presented in Figure 3b, it has been created using MatCont, and as such it is not validated globally but only locally near the bifurcation points.

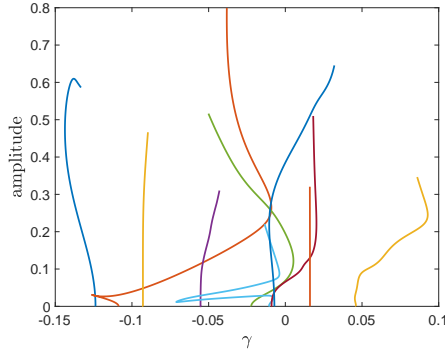
6 Outlook

In this work, we have initiated the automated rigorous study of validation methods for non-linear neural network dynamics. In a case study example, we have demonstrated the power of validation techniques to prove the existence of large numbers of periodic orbits, which can lead to complex oscillatory transients in the studied class of recurrent neural networks.

We briefly comment on potential, even more



(a) Bifurcation diagram associated with ODE



(b) An example of bifurcation diagram for a 20 dimensional system, with randomly generated matrices W and P and with seed 80.

Figure 3: Bifurcation diagrams. In these figures, the Hopf bifurcations are validated, while the periodic orbits are continued numerically from the bifurcation using MatCont. Here, we plot the parameter γ versus the amplitude of the periodic orbits.

general, applications for the rigorous validation paradigm. First, we could aim to study the learning process as a dynamical system, or even couple information propagation on the network with learning dynamics of the network (i.e., of its weights). The major obstacle in this context is not a primarily a conceptual one but a computational obstacle as the dynamical system for the weights grows quadratically in the dimension of the nodes. Second, we aim to validate in future work even more complex structures beyond periodic orbits and also tackle more global bifurcation curves. In these cases, also conceptual challenges can take center stage.

Acknowledgements: The reformulation (5) of algebraic Hopf bifurcation comes from a collaboration of Elena Queirolo with Jean-Philippe Lessard. CK and EQ would like to thank the VolkswagenStiftung for support via a Lichtenberg Professorship. EQ would like to thank the German Science Foundation (Deutsche Forschungsgemeinschaft, DFG) for support via a Walter-Benjamin Grant.

A Proving algebraic Hopf bifurcations

Given a vector $\phi \in \mathbb{R}^n$, the algebraic Hopf problem (5) is a zero finding problem

$$F : X = \mathbb{R} \times \mathbb{R} \times \mathbb{R}^n \times \mathbb{R}^n \times \mathbb{R}^n \quad (9)$$

$$\rightarrow Y = \mathbb{R} \times \mathbb{R} \times \mathbb{R}^n \times \mathbb{R}^n \times \mathbb{R}^n$$

$$(x, \gamma, \lambda_i, v_r, v_i)$$

$$\mapsto \begin{pmatrix} \phi^\top v_r \\ \phi^\top v_i - 1 \\ f(x, \gamma) \\ D_x f(x, \gamma) v_r + \lambda_i v_i \\ D_x f(x, \gamma) v_i - \lambda_i v_r \end{pmatrix}$$

where the space $X = Y$ is endowed with the Euclidean norm, thus making it a Banach space. In this paper, we are interested in

$$f(x, \gamma) = \tanh(\hat{W}(\gamma)x). \quad (10)$$

The Jacobian is defined in (3), and the algebraic Hopf zero-finding problem can be explic-

itly written as

$$\begin{aligned}
F(y) &= \begin{pmatrix} \phi^\top v_r \\ \phi^\top v_i - 1 \\ \tanh(\hat{W}(\gamma)x) \\ (\text{Id} - \text{diag}(\tanh(\hat{W}(\gamma)x^2)))\hat{W}(\gamma)v_r + \lambda_i v_i \\ (\text{Id} - \text{diag}(\tanh(\hat{W}(\gamma)x^2)))\hat{W}(\gamma)v_i - \lambda_i v_r \end{pmatrix} \\
&= 0
\end{aligned}$$

Let us assume we have a numerical solution $\hat{y} = (\hat{x}, \hat{\gamma}, \hat{\lambda}_i, \hat{v}_r, \hat{v}_i)$ to this zero finding problem.

Remark 3. Usually, iterative zero finding algorithms require a starting point y_0 in the neighborhood of a solution. For a general f , we can construct a rough approximation of the solution of (9) by fixing $\gamma = \gamma_0$ and finding x_0 numerically solving $f(x_0, \gamma_0) = 0$. In our case (10), we fix $\gamma_0 = 0$ and $x = 0$. Then, let $(\lambda_j, v_j), j = 1, \dots, n$ be all the eigenpairs associated to $D_x f(x_0, \gamma_0)$. A reasonable starting point is $y_0 = (x_0, \gamma_0, \text{Imag}(\lambda_0), v_0)$, where λ_0 is the eigenvalue closest to the imaginary axes and v_0 its associated eigenvector. Furthermore, the real part of λ_0 is a lower bound of the error. If such quantity is too large, the zero finding algorithm might diverge, and the initial choice of γ_0 should be reconsidered. In our case, any eigenpair can be chosen, since all of them cross the imaginary axes for an appropriate value of γ close to $\gamma_0 = 0$. Once a first approximation y_0 is found, the Newton's method can be used to return a sharper approximation \hat{y} .

With a numerical solution in hand, the radii polynomial approach is applied. We define A as a numerical inverse to $DF(\hat{y})$. Note how A is computed and stored numerically and does not need to be validated. Let $T(y) \stackrel{\text{def}}{=} y - AF(y)$, as in (6). We then compute

$$\|T(\hat{y})\|_X = \|AF(\hat{y})\|_X \leq Y.$$

By using Intlab on all computations, and all the computations being finite, the Y bound can be computed directly. The Z bound is more complicated and first requires a split-

ting. We use

$$\begin{aligned}
&\sup_{b, c \in B_1(0) \subset X} \|DT(\hat{y} + rb)rc\|_X \\
&= \sup_{b \in B_1(0) \subset X} \|\text{Id} - ADF(\hat{y} + rb)\|_{B(X, X)} r \\
&\leq \|\text{Id} - ADF(\hat{y})\|_{B(X, X)} + \sup_{b, c \in B_1(0) \subset X} \|ADF(\hat{y}) - ADF(\hat{y} + rb)\|_{B(X, X)} r
\end{aligned}$$

We then define

$$Z_1(r) = Z_1 r \geq \|\text{Id} - ADF(\hat{y})\|_{B(X, X)} r,$$

that can again be computed directly. For the second term, we apply the mean value theorem and get

$$\begin{aligned}
&\sup_{b \in B_1(0) \subset X} \|ADF(\hat{y}) - ADF(\hat{y} + rb)\|_{B(X, X)} r \\
&\leq \sup_{b, c \in B_1(0) \subset X} \|AD^2 F(\hat{y} + rb)rc\|_{B(X, X)} r.
\end{aligned}$$

A bound of this type can be achieved by computing the second derivative on the *interval* $\hat{y} \pm R$, where R is an *a priori* upper bound of the validation radius r^* . The interval notation is considered element-wise in all components of \hat{y} . In the same way, the vector c is replaced by the vector $\mathbf{1} \stackrel{\text{def}}{=} 0 \pm 1$, the vector having the interval $[-1, +1]$ in all coordinates. These modifications give

$$Z_2(r, R) = Z_2 r^2 \geq \|AD^2 F(\hat{y} \pm R)\mathbf{1}\|_{B(X, X)} r^2,$$

computed using interval arithmetic. Having constructed all the bounds, we need to find a value of r such that the radii polynomial $p(r) = Y + (Z_1 r + Z_2 r^2) - r$ is negative. This is an explicit computation since the radii polynomial is second order in r , giving

$$r_{\pm}^* = \frac{1 - Z_1 \pm \sqrt{(Z_1 - 1)^2 - 4Y Z_2}}{2Z_2}.$$

If such r_{\pm}^* exist, then the validation succeeded, and, for any r in the interval $[r_-^*, r_+^*]$, the ball centered at \hat{y} of radius r contains a unique solution.

In our case, this finishes the proof that an algebraic Hopf bifurcation is taking place at most r_-^* away from $(\hat{x}, \hat{\gamma})$.

B Proving non-degeneracy of Hopf bifurcations

This section is based upon standard results on Lyapunov coefficients presented in [33, Chapter 3] but we feel it is useful to explain in more detail, how non-degeneracy of Hopf is encoded within numerical validation techniques. A Hopf bifurcation (x_*, γ_*) of the ODE $x' = f(x, \gamma)$ is non-degenerate if there is a unique pair of imaginary eigenvalues of the Jacobian $D_x f(x_*, \gamma_*)$ and the first Lyapunov coefficient is non-zero. For the proof of this statement we refer to [33]. In this section, we define the first Lyapunov coefficient constructively, such that its validated computation can conclude the proof of the non-degeneracy of a Hopf bifurcation.

Let $x' = f(x, \gamma)$ be a parameter-dependent ODE, as in Section 3, with $x \in \mathbb{R}^n$, $\gamma \in \mathbb{R}$, and let (x_*, γ_*) be an algebraic Hopf bifurcation. Let J be the Jacobian $D_x f(x_*, \gamma_*)$, having a unique pair of purely imaginary eigenvalues. Let $i\lambda$ be the positive imaginary eigenvalue of J . Then, let v be the eigenvector of J associated to $i\lambda$, and let w be the eigenvector of J^\top associated to $-i\lambda$. Notice how both v and w are defined up to a complex constant. We introduce the complex inner product

$$\langle x, y \rangle \stackrel{\text{def}}{=} \bar{x}^\top y,$$

and we request $\langle v, v \rangle = 1$ and $\langle v, w \rangle = 1$. This rescaling is not necessary to determine the sign of the first Lyapunov coefficient, and could be skipped, as long as $\langle v, w \rangle > 0$. Then, the first Lyapunov coefficient is defined as

$$l_1 = \frac{1}{2\lambda^2} \text{Real}(i\langle w, D^2 f(x_*, \gamma_*)vv \rangle + \langle w, D^2 f(x_*, \gamma_*)v\bar{v} \rangle + \lambda\langle w, D^3 f(x_*, \gamma_*)vv\bar{v} \rangle).$$

Each derivative of order k is considered as an operator acting on k elements of \mathbb{R}^n .

Having built in the previous Section A an error bound of x_* and γ_* , we use the Intlab eigenpair validation functionality to build a validated interval for λ , v and w and then we compute l_1 explicitly. If the validated interval

of existence for l_1 does not contain 0, the proof of the non-degeneracy of the Hopf bifurcation is completed. In the examples provided, the majority of non-degeneracy validations were successful.

References

- [1] E. Alpaydin. *Introduction to Machine Learning*. MIT Press, 2020.
- [2] K.P. Murphy. *Machine Learning: a probabilistic perspective*. MIT press, 2012.
- [3] B. Schölkopf and A.J. Smola. *Learning with Kernels: support vector machines, regularization, optimization, and beyond*. MIT Press, 2001.
- [4] M.I. Jordan and T.M. Mitchell. “Machine learning: Trends, perspectives, and prospects”. In: *Science* 349.6245 (2015), pp. 255–260.
- [5] D. Silver et al. “Mastering the game of Go with deep neural networks and tree search”. In: *Nature* 529.7587 (2016), pp. 484–489.
- [6] Y. LeCun, Y. Bengio, and G. Hinton. “Deep learning”. In: *Nature* 521.7553 (2015), pp. 436–444.
- [7] J. Schmidhuber. “Deep Learning in Neural Networks: An Overview”. In: *Neural Networks* 61 (2015), pp. 85–117.
- [8] A. Pinkus. “Approximation theory of the MLP model in neural networks”. In: *Acta Numer.* 8 (1999), pp. 143–195.
- [9] F. Scarselli and A.C. Tsoi. “Universal approximation using feedforward neural networks: A survey of some existing methods, and some new results”. In: *Neural Networks* 11.1 (1998), pp. 15–37.
- [10] W. E. “A proposal on machine learning via dynamical systems”. In: *Commun. Math. Stat.* 5.1 (2017), pp. 1–11.
- [11] J.D. Farmer, N.H. Packard, and A.S. Perelson. “The immune system, adaptation, and machine learning”. In: *Phys. D* 22.1 (1986), pp. 187–204.

- [12] J. Guckenheimer and P. Holmes. *Nonlinear Oscillations, Dynamical Systems, and Bifurcations of Vector Fields*. New York, NY: Springer, 1983.
- [13] W. De Melo and S. Van Strien. *One-dimensional Dynamics*. Springer, 2012.
- [14] T.D. Sanger. “Optimal unsupervised learning in a single-layer linear feedforward neural network”. In: *Neural Networks* 2.6 (1989), pp. 459–473.
- [15] M.N. Galtier and G. Wainrib. “Multiscale analysis of slow-fast neuronal learning models with noise”. In: *J. Math. Neurosci.* 2 (2012), p. 13.
- [16] C. Kuehn. *Multiple Time Scale Dynamics*. Springer, 2015.
- [17] S. Mei, A. Montanari, and P.A. Nguyen. “A mean field view of the landscape of two-layer neural networks”. In: *Proc. Natl. Acad. Sci. USA* 115.33 (2018), E7665–E7671.
- [18] T. Tanaka. “Mean-field theory of Boltzmann machine learning”. In: *Phys. Rev. E* 58.2 (1998), p. 2302.
- [19] L. Ambrosio, N. Gigli, and G. Savaré. *Gradient Flows: In Metric Spaces and in the Space of Probability Measures*. Birkhäuser, 2006.
- [20] S. Wang, V. Teng, and P. Perdikaris. “Understanding and mitigating gradient flow pathologies in physics-informed neural networks”. In: *SIAM J. Sci. Comput.* 43.5 (2021), A3055–A3081.
- [21] Yu. Ilyashenko. “Centennial history of Hilbert’s 16th problem”. In: *Bull. Amer. Math. Soc.* 39.3 (2002), pp. 301–354.
- [22] G. Arioli and H. Koch. “Computer-assisted methods for the study of stationary solutions in dissipative systems, applied to the Kuramoto–Sivashinski equation”. In: *Arch. Rat. Mech. Anal.* 197.3 (2010), pp. 1033–1051.
- [23] J.P. Lessard S. Day and K. Mischaikow. “Validated continuation for equilibria of PDEs”. In: *SIAM J. Numer. Anal.* 45.4 (2007), pp. 1398–1424.
- [24] T. Kapela et al. “CAPD:: DynSys: a flexible C++ toolbox for rigorous numerical analysis of dynamical systems”. In: *Commun. Nonl. Sci. Numer. Simul.* 101 (2021), p. 105578.
- [25] J.B. van den Berg, J.D.M. James, and C. Reinhardt. “Computing (un)stable manifolds with validated error bounds: non-resonant and resonant spectra”. In: *J. Nonlin. Sci.* 26.4 (2016), pp. 1055–1095.
- [26] W. Tucker. “The Lorenz attractor exists”. In: *C.R. Acad. Sci. Paris* 328 (1999), pp. 1197–1202.
- [27] Bo Chang et al. “AntisymmetricRNN: A dynamical system view on recurrent neural networks”. In: *arXiv preprint arXiv:1902.09689* (2019). URL: <https://arxiv.org/pdf/1902.09689.pdf>.
- [28] Christian Kuehn and Elena Queirolo. *Code for “Computer Validation of Neural Network Dynamics: A First Case Study”*. https://drive.google.com/file/d/1b6Mizsf_AEXXGx01L. 2022.
- [29] Allan Hungria, Jean-Philippe Lessard, and Jason D Mireles James. “Rigorous numerics for analytic solutions of differential equations: the radii polynomial approach”. In: *Mathematics of Computation* 85.299 (2016), pp. 1427–1459.
- [30] Jean-Philippe Lessard, JD Mireles James, and Julian Ransford. “Automatic differentiation for Fourier series and the radii polynomial approach”. In: *Physica D: Nonlinear Phenomena* 334 (2016), pp. 174–186.
- [31] Maxime Breden, Jean-Philippe Lessard, and Matthieu Vanicat. “Global bifurcation diagrams of steady states of systems of PDEs via rigorous numerics: a 3-component reaction-diffusion system”. In: *Acta applicandae mathematicae* 128.1 (2013), pp. 113–152.

- [32] Siegfried M Rump. “INTLAB—interval laboratory”. In: *Developments in reliable computing*. Springer, 1999, pp. 77–104.
- [33] Yuri A Kuznetsov. *Elements of applied bifurcation theory*. Vol. 112. Springer Science & Business Media, 2013.
- [34] Annick Dhooge, Willy Govaerts, and Yu A Kuznetsov. “MATCONT: a MATLAB package for numerical bifurcation analysis of ODEs”. In: *ACM Transactions on Mathematical Software (TOMS)* 29.2 (2003), pp. 141–164.
- [35] Jan Bouwe Van den Berg, Jean-Philippe Lessard, and Elena Queirolo. “Rigorous verification of Hopf bifurcations via desingularization and continuation”. In: *SIAM Journal on Applied Dynamical Systems* 20.2 (2021), pp. 573–607.
- [36] Chris M Groothedde and JD Mireles James. “Parameterization method for unstable manifolds of delay differential equations”. In: *Journal of Computational Dynamics* 4.1&2 (2017), p. 21.